ELSEVIER

Geotextiles and Geomembranes 14 (1996) 585–600

0266-1144/96 $15.00

PII: S0266-1144(96)00043-X

Perforation Strength of Geosynthetics and Sphericity of Coarse Grains: a New Approach

R. Antoine & L. Courard

Department of Construction Materials, Institute of Civil Engineering, University of Liège, quai Banning 6, 4000 Liège, Belgium

ABSTRACT

Perforation of a geomembrane by the coarse grains in the drainage layer of a composite liner for a landfill would be a serious environmental problem. Therefore, the geomembrane is generally protected against perforation by a geotextile. Several laboratory tests already exist for designing the geotextile. Some of them use coarse grains as penetrators, others replace them by artificial geometrically defined penetrators. The first method has the disadvantage of not being reproducible while the second method lacks any correlation between the morphology of the stones and the form of the penetrators.

A method of correlating the form of the penetrators with that of the stones has been established (Antoine, 1995). It is based on the measurement of the angularity and bluntness of the bumps on the stones. These measurements were made by analysing digitised pictures. A probability analysis using the Beta law has been used to define the angles and bluntness characterising a 'dangerous' stone and an 'average' stone. Then, steel penetrators were manufactured with these characteristics.

Puncture tests have been run with these artificial penetrators to compare the efficiency of some protection geotextiles. Other tests using stones as penetrators have then been performed to verify the effectiveness of the simulation of the coarse grains. It seems that the correlation found is valid, but that another parameter, describing the more general form of the stone around the bump, is necessary to explain the differences in behaviour. © *1997 Elsevier Science Ltd. All rights reserved.*

1 INTRODUCTION

Geomembranes used in waterproofing systems are subjected to strains and deformations which can vary in the extreme from one point to another. The

main role of the geomembrane is to guarantee the waterproofing and any loss of this property could have very serious consequences. Therefore, the geomembrane is generally protected by a 'cushioning' geotextile. This has to be designed in order to secure the durability of the waterproofing by absorbing the more extreme strains induced by the loads above the drainage layer.

Different kinds of tests have already been developed to determine the bursting and perforation strength of geomembranes, geotextiles and systems made of a combination of both. The cone drop test (Belgian Ministry for Public Works) involves measuring the effect of a conical mass falling onto the geotextile. This test allows a comparative classification of different products but lacks a quantified measurement of their strength. The large tank test with original drainage material (Rigo, 1978) and the plate load test also using the original drainage layer (Saathoff & Sehrbrock, 1994) allow the study of the behaviour of protected or unprotected geomembranes under loading (hydraulic pressure and a compressed ballast, respectively). Unfortunately, the data obtained from such puncture tests using original drainage material show scattering over a wide range because the arrangement of the natural gravel is random and varies from test to test.

To remedy scattering, geometrically defined penetrators have been used in place of the natural gravels. It is for this reason that tests such as the large tank test using a group of pyramids as penetrators (Rigo, 1978), the CBR puncture test (Brummermann *et al.*, 1993; Saathoff & Sehrbrock, 1994) and the plate penetrator test (Brummermann *et al.*, 1994) have been developed. The first quantifies the limiting hydraulic load above the geomembrane, the second quantifies the perforation strength of the geosynthetic for a single bump; and the third is as for the previous test but uses a bed of bumps. However, in these tests, the form, surface condition and position of the

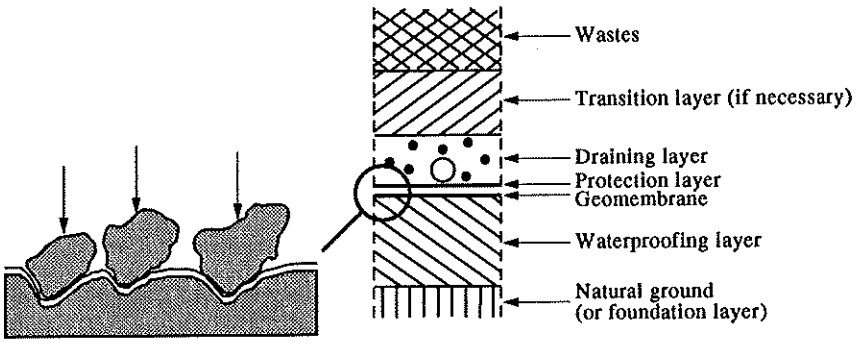

Fig. 1. Cross-section of a classical waterproofing drainage system for landfills.

TABLE 1
Results from analysis of the stones

	Crushed		*Rounded*	
	Dangerous	*Average*	*Dangerous*	*Average*
Angularity (°)	35·1	79·3	48·5	88·2
Bluntness (mm)	0·6	2·4	1·2	3·6

penetrators have all been chosen by trial and error in the hope of reproducing the results from the tests using natural stones. In this research, we have established a new systematic method which allows proper design of the penetrators used to simulate the stones, depending on the characteristics of the coarse grains (granular size, elongation, coarseness, angularity and bluntness).

2 DEVELOPMENT OF THE PENETRATORS

2.1 Method for analysis of the gravels

The method selected as being the most robust and the most objective is based on calculating several characteristics from a digitised picture of the stone. The picture being the projected shadow of the stone laid to show its most pronounced bump. Such pictorial analysis is probably the only tool able to give detailed morphometric information about every individual stone (Pirard, 1994). The word 'morphology' is used in this context as the discipline which measures form.

By means of transformations from morphologic mathematics a strict form descriptor named 'Calyptre' has been found. It links every outline point of the stone with the radius and the centre of the largest inscribable circle and the tangent to the outline in this point. These measurements are automatically calculated by the picture analysis. The pictures are recorded by a black and white camera and then digitised into a 512 × 512 8-bit picture (Pirard, 1990). In this work, the need to maximise the stone size and the limitations of the optical device resulted in the average number of pixels being about 6000.

Several independent parameters are used to characterise the form, each defining an overall characterisation or a more local characterisation of the stone. These parameters are the stone's elongation, equivalent bluntness and overall coarseness, together with the bluntness and angularity of the individual bumps.

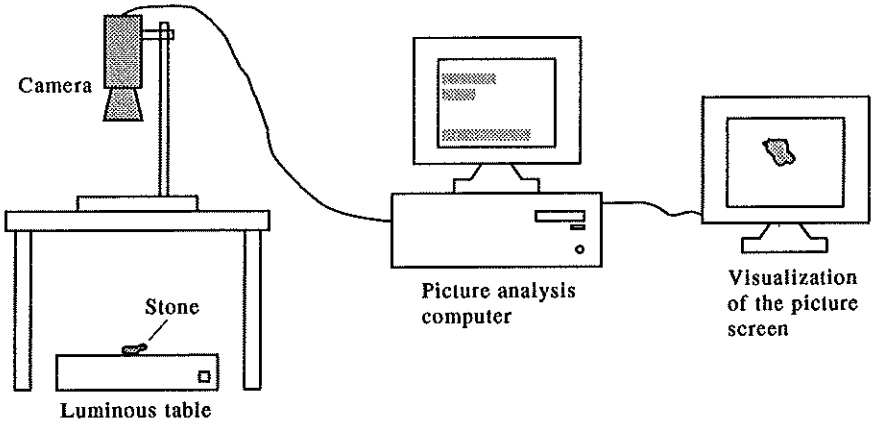

Fig. 2. Schematic view of the device used for the pictorial analysis.

The elongation: this is found by an automatic search routine which projects the object onto a series of given orientation straight lines. The semi-major and the semi-minor axes of the ellipse with the equivalent moment of inertia are used to calculate the elongation.

The global coarseness: this measurement quantifies the relative importance of the area within the bumps. A rigorous definition of what rough or smooth is in this context is needed. A fixed mathematical definition of a smooth reference surface may be given by the notion of the Moderate Ultimate Homotopic Insertion (MUHI). The ultimate insertion is the set resulting from a λ_E size insertion (λ_E is the radius of the largest inscribable circle in the form). A λ size insertion is the area which can be covered by an inscribed circle of radius λ.

So, the global coarseness is given by the following formula:

$$R_G^v = \frac{A[X - \mathrm{MUHI}(X)]}{A[X]}$$

where $A[X]$ is the total plan area of stone X, $A[\mathrm{MUHI}(X)]$ is the plan area covered by the MUHI circles, and hence $A[X - \mathrm{MUHI}(X)]$ corresponds to the black area in Fig. 3.

The bluntness and the angularity: in practice, a bump can be characterised by the measurement of its bluntness and angularity. The bluntness of a bump is usually defined as

$$W_i = \frac{\lambda_{xi}}{\lambda_E}$$

where λ_{xi} is the radius of the inscribed circle at the end of bump i of stone x; λ_E is the radius of the largest inscribable circle. However, in our situation, we

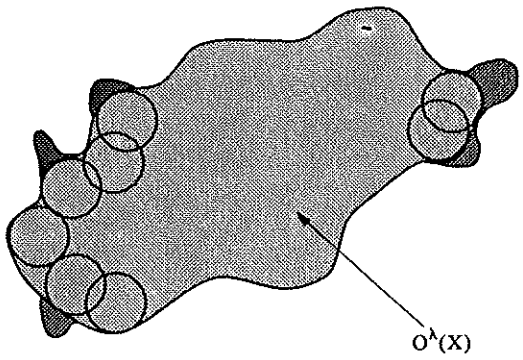

Fig. 3. Morphologic insertions of an object by a λ circle. The areas missed by the insertions (in black) correspond to the coarseness.

have used the notion of bluntness defined solely by the radius of the circle inscribed at the end of the bump (λ_x).

The angularity is given by

$$\hat{S}_i = 2 \arcsin\left(\frac{\lambda_{u_i} - \lambda_{x_i}}{d_{ux_i}}\right)$$

where λ_{u_i} is the radius of the circle at the base of the bump; d_{ux_i} is the distance between the centre of the base circle and the centre of the end circle.

The base circle radius is defined to be the first λ value, on each side of λ_{xi}, which is either a local maximum or higher than λ_m (which belongs to the smooth reference).

In practice, each stone is characterised by measurements of bluntness and angularity for each bump.

The equivalent bluntness: this parameter more or less gives the equivalent bluntness of the stone's entire outline using the relative curvature at each outline point. The equivalent bluntness W_v is given by the following formula

$$W_v = \frac{1}{\sqrt{\overline{V} - 1}}$$

where $\overline{V}$ is the average abrasion parameter given by

$$\overline{V} = \frac{1}{N} \sum_{i=1}^{N} \left[1 + \frac{\lambda_E}{\lambda_i}\right]^2$$

where N is the number of points along the outline; λ_E is the radius of the largest inscribable circle into the outline; λ_i is the radius of the largest inscribable circle at point i.

In order to appreciate the effectiveness of the method, two kinds of gravels

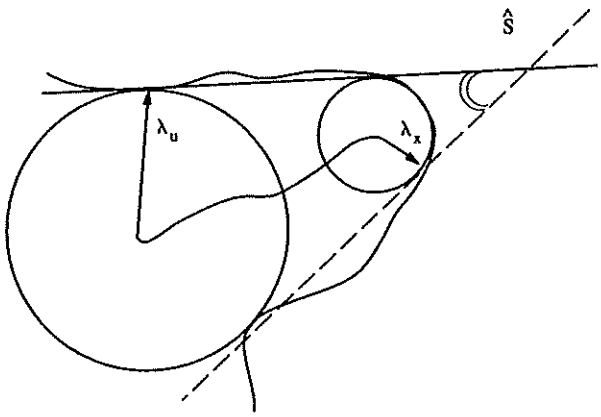

Fig. 4. Geometrical construction used to calculate the angularity of a given bump.

have been analysed, one with rounded grains and the other with crushed grains. The granular size was restricted by the availability of material and the limitations of the picture analysis device. A size of 14/28 mm was selected for the rounded grains. The PSD (particle size distribution) curve of the crushed grains was reconstituted to be the same as that of the rounded grains. This reconstitution eliminated any effect on the results due to the grading parameters.

The number of stones analysed was fixed at 200 for each kind of gravel because it was found that the results did not vary when this number was increased. Due to the need for convergence in the image analysis process, angularity and bluntness were limited to 120° and 50%, respectively. These values were chosen because they were low enough to be effective without any significant influence on the design of the artificial penetrators. Moreover, any error is on the safe side as it shifts the probability results towards the more damaging small angles and sharper bluntness values (Figs 5 and 6). In this first approach, only angularity and bluntness effects have been studied.

2.2 Granular characteristic analysis

The largest puncture risk is certainly posed by a stone which presents at the same time the sharpest bluntness and the smallest angularity. However, the probability of having such a stone is very minimal because there are few results in the left lower corner of Figs 5 and 6. Moreover, we should take into account the probability of having this stone in contact with the geosynthetic and with the bump being in the worst position. Such a situation is extremely rare and can be considered as improbable. However, the risk of puncture does not come from 'average' stones. A design based on such

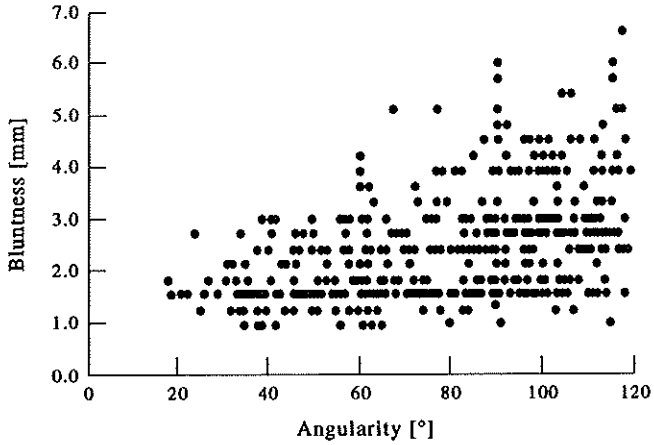

Fig. 5. Resulting couples (α_i, λ_i) for crushed grains.

stones is far from safe and cannot be used. The solution is a compromise between these two extreme situations. In practice, it is logical to think that a 'dangerous' stone would be surrounded by a large number of 'average' stones. Now, the task is to determine what is a 'dangerous' stone.

The above problem was solved using a probability approach. The number of results (several hundred) justifies the use of a Beta law (Bolle, 1992). This law is able to represent a large range of distribution forms from the values of the first four moments. To use it in our case, the resulting couples (α_i, λ_i) have to be referenced to only one variable Z by projecting the experimental points onto the average regression line of equation $\lambda - \bar{a}\alpha + \bar{b}$ passing through the average point ($\alpha_{average}$, $\lambda_{average}$). The variable Z is defined as the abscissa of the projection of the couples (α_i, λ_i) onto this line.

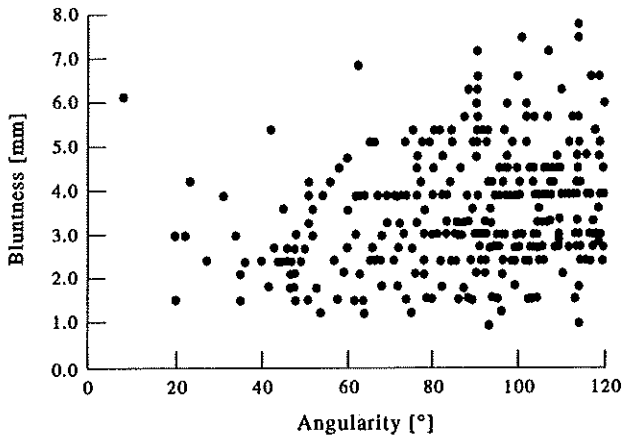

Fig. 6. Resulting couples (α_i, λ_i) for rounded grains.

TABLE 2
Geotextile characteristics

Test	*Unit*	*W1*	*W2*	*NW1*	*NW2*	*NW3*	*NW4*
Mass per unit area	g/m^2	385	825	850	1240	2270	1700
Resistance CBR	N		10000	5300	6500	11000	8000
Breaking strength							
Warp	kN/m	80	200	50	57	85	35
Weft	kN/m	80	100	32	36	52	40
Breaking elongation							
Warp	%	15	30	90	80	90	35
Weft	%	8	10	140	120	140	20

The application of the Beta law to this variable Z allows the identification of an angularity $\alpha_{\text{dangerous}}$ and a bluntness $\lambda_{\text{dangerous}}$ corresponding to the characteristics of a 'dangerous' stone. This pair of values is selected so that the probability of a set of higher, less damaging, values is 95%. The previous

TABLE 3
Test results for the C penetrator plate simulating the crushed grains

Protection geotextile	*Perforation load* (N)	*Perforation pressure* (bars)
/	3000	9·6
/	3100	9·9
/	3500	11·2
/	2900	9·3
/	3350	10·7
W1	6550	21·0
W1	5700	18·3
W1	6500	20·9
W2	7700	24·7
W2	7200	23·1
W2	7100	22·8
NW1	10400	33·4
NW1	< 12800	< 41·1
NW1	10800	34·6
NW2	15000	48·1
NW2	16000	51·3
NW2	< 19000	< 61·0
NW3	17000	54·5
NW3	< 25000	< 80·2
NW3	12600	40·4
NW4	< 25000	< 80·2
NW4	25200	80·8

developments enabled the following characteristic for the angularity and bluntness of the rounded and crushed grains to be obtained.

The first tests were performed using steel penetrator plate (C) which simulates the crushed grains. The last column gives the pressure in bars corresponding to the load on the penetrator plate surface. It is given by

$$P = \frac{L}{A}$$

with P the pressure in bars, L the load in N, A the are of the base plate to the penetrators.

2.3 Penetrator plate design

The pictorial analysis gives only bidimensional information on the bumps. The aim of this first approach is limited to the simulation of the angularity and bluntness and therefore a conical form was chosen for the penetrators. The dangerous penetrator is surrounded by average penetrators as explained above because this is a more probabilistic view of the reality. In order to keep some circular symmetry and a plausible arrangement, the penetrators were set as presented in Fig. 7. The distance between the summits is fixed to the d_{50} value from the PSD curve of the gravel (in this case $d_{50} = 21$ mm). This value also fixes the penetrator's height.

3 THE PUNCTURE TEST

A realistic test to simulate geomembrane–geotextile perforation by the drainage layer can be performed using the above penetrator plate to load the system. The test device is composed of a watertight tank filled with the

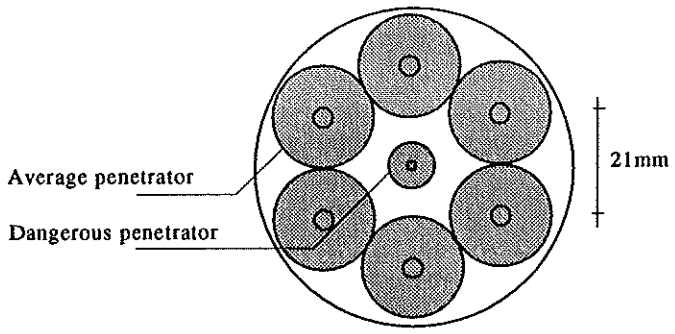

Fig. 7. Plan view of a penetrator plate.

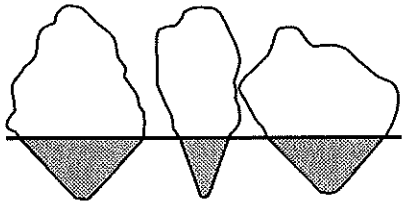

Fig. 8. Cross-section of the penetrator plate.

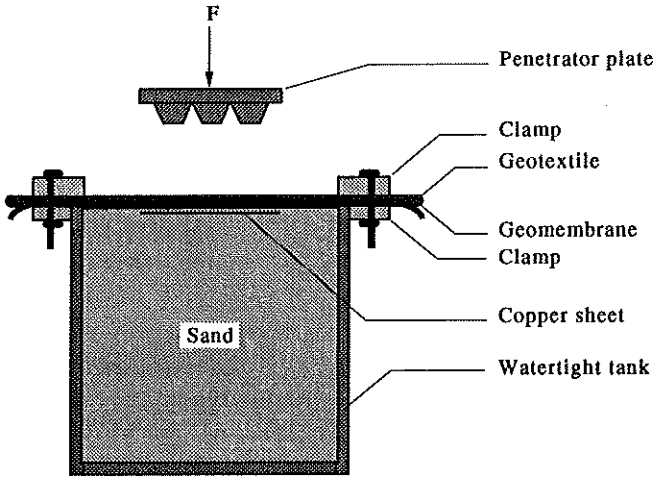

Fig. 9. Schematic view of the testing device.

support soil which was in this case sand instead of clay. The geomembrane and the geotextile are placed above this and fixed to the tank with a bolted clamp. The loading is applied by a rigid plate on which the penetrators are determined by the simulated stone characteristics.

Some test and apparatus values:

TABLE 4
Test results for the C penetrator plate simulating the rounded grains

Protection geotextile	*Perforation load* (N)	*Perforation pressure* (bars)
/	7000	22·4
W1	12 550	40·3
W1	13 000	41·7
W2	17 500	56·1
NW1	28 750	92·2
NW2	30 750	98·6

- Speed of loading: 2 mm/min.
- Inside diameter of the tank: 35 cm.
- Outside diameter of the clamp: 50 cm.
- Thickness of the copper sheet: 40 μm.

The tests were performed on a range of different geotextiles using two different penetrator plates. In each test the load was steadily applied until perforation was detected using an electrical method.

The analysis attempts to relate the penetration load to the geotextile type and the mass per unit area.

4 PUNCTURE TESTS RESULTS

The geomembrane used in the tests was a HDPE 2 mm thick geomembrane. Six geotextiles were tested: two wovens (W1, W2) and four nonwovens (NW1, NW2, NW3, NW4).

Two further tests were performed with penetrator plate C, but without any geotextile, and with the central cone replaced with a representation of an 'average' stone. A significant increase in the breaking load (between 16 000 and 17 000 N instead of 3200 N with the 'dangerous' cone) was observed.

Then, the R penetrator plate simulating the rounded grains was used. Geotextiles NW3 and NW4 could not be tested because the perforation load exceeded that which could be applied by the test apparatus.

The results for penetrator plates C and R are presented in Figs 10–12. These Figures suggest that there is a linear relation between the mass per unit area of the geotextile and the puncture strength of the system.

It can be observed that:

- With the R plate, the perforation loads are more than twice those with the C plate, and this applies to both woven and nonwoven geotextiles: i.e. $L_R \geqslant 2\,L_C$.
- Nonwovens permit, for the same mass per unit area, a 30% higher protection than with the wovens, and that for each penetrator plate $L_{\text{nonwovens}} \geqslant 1{\cdot}3\,L_{\text{wovens}}$. This is due to the fact that, in our case, the support soil is perfectly flat without any bumps and the geotextile thickness plays a basic role by absorbing a large part of the strains before they have an impact on the geomembrane.
- Wovens have the disadvantage that the bumps could penetrate the geotextile by separating the perpendicular warp and weft fibres.
- For the woven geotextiles, the increase in penetration load with the mass per unit area is 2·44 times greater for the rounded penetrator R than for the crushed penetrator C; and for the nonwovens this ratio is 2·35.

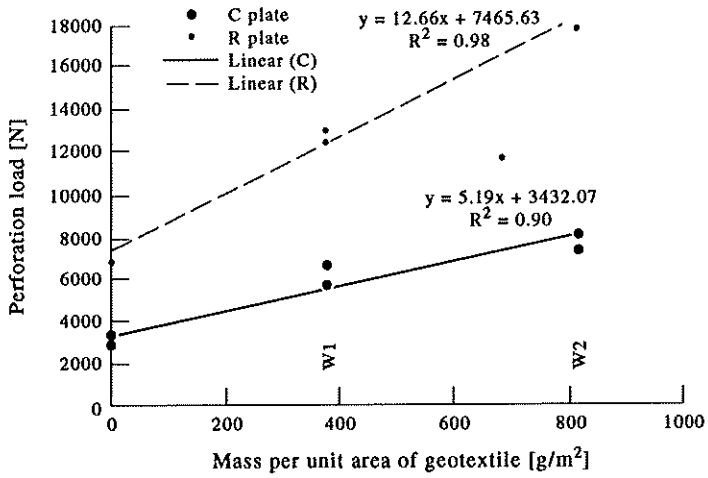

Fig. 10. Regression lines for the perforation load of the woven geotextiles tested with artificial penetrator plates C and R.

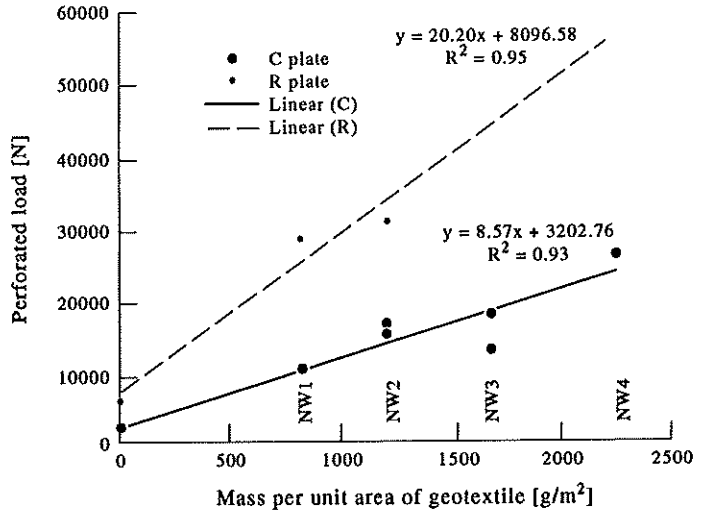

Fig. 11. Regression lines for the perforation load of the nonwoven geotextiles tested with artificial penetrator plates C and R.

- The geomembrane alone, without any protection, when tested with the R penetrator plate is able to resist up to 2·2 times the penetration load for the C penetrator plate

The comparison of the woven and nonwoven geotextiles when tested with C and R penetrators is illustrated in Fig. 12.

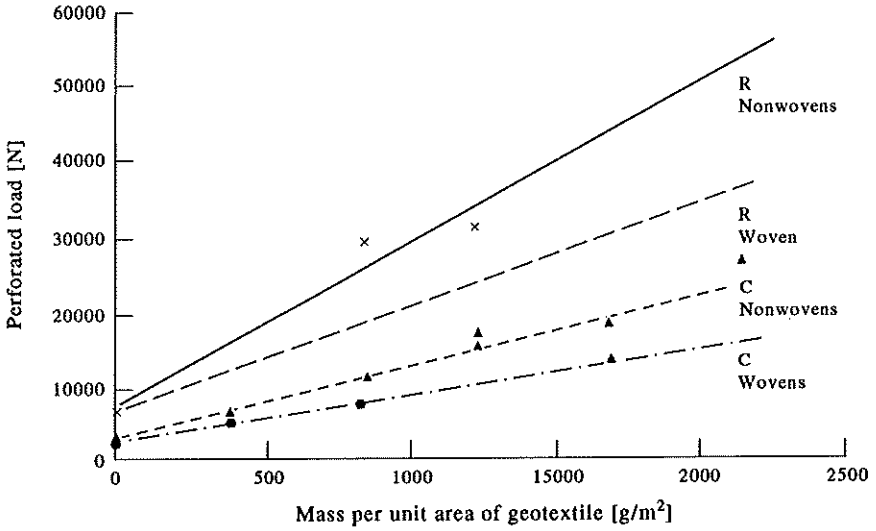

Fig. 12. Comparison between the results of woven and nonwoven geotextiles.

Lastly, comparative tests using natural stones as penetrators were undertaken. In order to secure some repeatability for these tests, the stones were embedded in a resin mortar with the same arrangement as used on the C and R penetrator plates. Only the woven geotextiles could be tested because the loads reached with the nonwovens were so high that the stones broke, crumbled away or became loose.

The following results were obtained using the crushed gravels (CG1 and CG2).

Figure 13 shows that the perforation load increases with the mass per unit area of the geotextile. However, the trend is less linear than observed with

TABLE 5
Results of the tests using crushed gravel as the penetrator

Penetrator name	*Protection geotextile*	*Perforation load* (N)	*Perforation pressure* (bars)
CG1	/	8500	27·3
CG1	/	8000	25·7
CG2	/	6500	20·8
CG2	/	7000	22·4
CG1	W1	13 000	41·7
CG2	W1	12 500	40·1
CG1	W2	13 500	43·3
CG2	W2	12 000	38·5

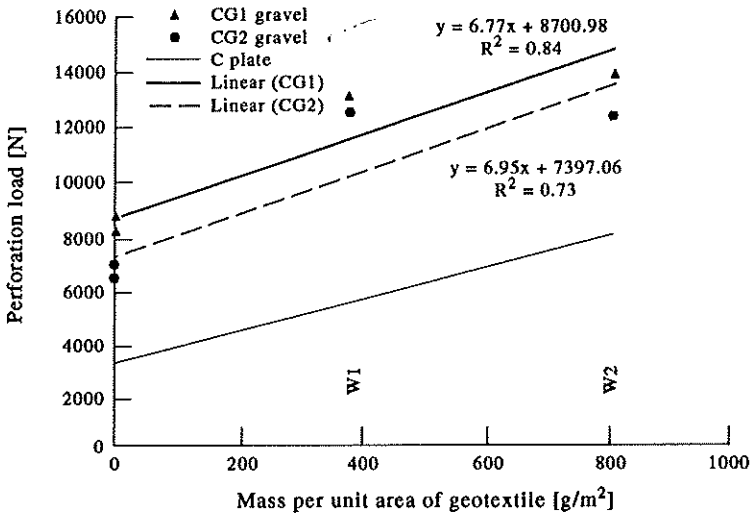

Fig. 13. Perforation load for the woven geotextiles tested with penetrators of crushed gravels CG1 and CG2.

the artificial penetrator plate C, showing a more gradual improvement at the higher values of mass per unit area.

It is observed that the trends obtained for CGI and CG2 are roughly parallel to that obtained with the C penetrator plate. The fact that the results from the artificial penetrator are lower proves that the proposed simulation method is safe.

The reduction in the linearity of the last results can be explained as follows. For the lighter geotextiles, puncture is very dependent on the tip of the penetrator. For the thicker geotextiles the zone around the tip starts to become important. Unlike the artificial penetrators which only simulate the bump (by its angularity and its bluntness), the natural stones induce the whole form effect including the relief around the bump.

When the indentation reaches a certain value the geomembrane–geotextile system touches the sides of the bump, reducing the importance of the tip.

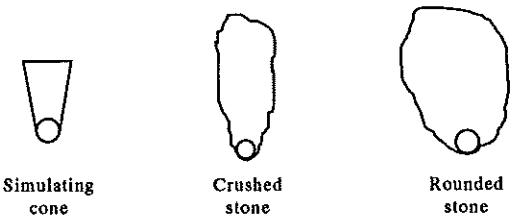

Fig. 14. Comparison of the relief around the bump for the cones, crushed stones and rounded stones.

The penetrating break now depends more on the stretch of the geomembrane on the sides of the bump than on the shape of the bump.

To take into account this phenomenon, a third parameter should be defined in the analysis of the stones. This parameter would describe the more general form around the bump of the stone.

5 CONCLUSIONS

The perforation of geosynthetics used in composite waterproofing drainage layers for waste storage is clearly a problem. There is a need to correctly design the perforation protection, particularly according to the granular size and the morphology of the coarse grains used for the drainage layer.

Simulation of the coarse grains by artificial penetrators used in penetration tests on a geomembrane protected or not with geotextiles permitted us to conclude that:

- the morphology of the grains, defined in terms of elongation, global coarseness, equivalent bluntness, angularity and bluntness of individual bumps, is sufficient to define the shape of the grain and can be clearly correlated with an artificial simulation.
- It is possible to define, by means of the probability analysis, 'dangerous' and 'average' stones.
- It is possible to take into account the PSD of the stones by means of the geometric disposition of the artificial penetrators.

From the tests performed it was observed that:

- With the penetrator plate which simulated the rounded grains, the perforation loads are more than twice those with the plate simulating crushed grains and this applies to both woven and nonwoven geotextiles.
- The use of nonwoven geotextiles permits, for the same mass per unit area, a 30% higher protection than with the wovens, and that applied to both penetrator plates.
- Tests using natural stone penetrators confirmed these patterns of behaviour.
- Tests using natural stone penetrators gave higher penetration loads than for the artificial penetrators, confirming the method of simulating the gravels was safe.

Nevertheless, the reduced linearity in the results from this last kind of test indicates that the more general form of the stone around the bump can be significant, suggesting the possible need for another parameter in the design of the artificial penetrators.

Further studies are currently underway using other tests to investigate the following aspects:

- To take into account a parameter related to more general sphericity of the stone to explain the differences in the results for the heavier geotextiles.
- To test the method for larger granular sizes.
- To try to find a relation between the local stretch of the geomembrane, the amount of indentation and the load.

6 REFERENCES

Antoine, R. (1995). Travail de fin d'études: Résistance à la perforation des géosynthétiques et sphéricité des granulats: une nouvelle approche, Université de Liège.

Bolle, A. (1992–1993). Cours: Méthodes probabilistes en infrastructure, Université de Liège.

Brummermann, K., Kohlhase, S. & Saathoff, F. (1993). Puncture loads on geomembranes in composite liners. *Fourth International Landfill Symp.*, Cagliari, Italy, pp. 357–367.

Brummerman, K., Blumel, W. & Stoewahse, C. (1994). Protection layers for geomembranes: effectiveness and testing procedures. *Fifth International Conf. on Geotextiles, Geomembranes and Related Products*, Singapore, Vol. 3, pp. 1003–1006.

Ministere des Travaux Publics, Services Techniques Généraux; Circulaire 576N.M./6, Emploi des Géotextiles (reprise dans la norme NBN B29001).

Pirard, E. (1990). Applications of shape analysis in ore benefication. *Process Mineralogy IX*. The Minerals, Metals & Materials Society.

Pirard, E. (1994). Analyse morphométrique des poudres: une approche systématique et robuste par la morphologie mathématique. *La Revue de Métallurgie–CIT/Science et Génie des Matériaux*, February.

Rigo, J. M. (1978). Corrélation entre la résistance au poinçonnement sur ballast et les caractéristiques mécaniques des membranes détanchéité. *Matériaux et Constructions; Essais et Recherches*, No. 65.

Saathoff, F. & Sehrbrock, U. (1994). Indicators for selection of protection layers for geomembrane. *Fifth International Conf. on Geotextiles, Geomembranes and Related Products*, Singapore, Vol. 3, pp. 1019–1022.